*Velmurugan. Amirthavalli[1], Anita R. Warrier[2]**

[1]Department of Petroleum Engineering, [2]Nanophotonics Research Laboratory, Department of Physics, Academy of Maritime Education and Training, Chennai, Tamilnadu, India

Scientific paper
ISSN 0351-9465, E-ISSN 2466-2585
https://doi.org/10.62638/ZasMat1331

Zastita Materijala 66 ( )
(2025)

Investigation of structural, optical, and emission properties of SnO_2 nanoparticles by thermal decomposition method

ABSTRACT

SnO_2 nanoparticles were synthesized usingthe thermal decomposition technique by varying the temperature from 300˚C to 600˚C. The synthesized nanoparticles (9 nm) were of rutile (tetragonal) phase with orientation along [110], [101], [200], [211], [220], [310], [112], [301], [202]crystal planes. The peak intensity of the crystal planes becomes prominent with an increase in decomposition temperature while the impurity phases diminish. The nanoparticle's crystallite size and microstrain were calculated using the William Hall equation with the union deformation model. SnO_2 nanoparticles synthesized at 600˚Cshow a positive strain of 0.3571x10^{-3}indicates lattice expansion. At thermal decomposition of 500 ^{0}C, the sample has maximum transparency with a band gap at ~ 4.19 eV and broad emission in the blue region of the EM Spectra with high intensity (5 x10^5 counts), rendering it suitable for blue light LEDs.

Keywords: *Thermal decomposition method**,**SnO_2Nanoparticles, Tin(II) chloride dihydrate*

1. INTRODUCTION

Tin oxides normally exist in stannic oxide (SnO_2-cassiterite) and stannous oxide (SnO -SnO-romarchite) forms and occasionally in the Sn_3O_4 and Sn_2O_3phases. SnO is metastable at ambient conditions and gets converted into SnO_2 by oxidation whereas $SnO_2$is highly stable [1]. $SnO_2$is ann-type crystalline semiconductor havinga direct optical transition band gap of ~ 3.6eV–3.8 eV[2] or an indirect transition of~ 2.7eV-3.1 eV, with a rutile ($P4_2/mnm$) tetragonal shape (lattice parameters of a = 4.738 Å and c = 3.187 Å).SnO_2exists in various polymorphs such as $CaCl_2$-type (Pnnm), α-PbO_2-type (Pbcn), pyrite-type (Pb3), ZrO_2-type orthorhombic phase I (Pbca), and fluorite-type (Fm3m) [3-5] and has melting point of 1127°C and an exciton binding energy of 1300 meV (at 293 K) [6].

SnO_2 can be synthesized in various forms such as nanoparticles, nanorods, nanobelts, nanotubes, hollow microspheres, nanoflowers [7,8], mesoporous structures, nanosheets [9,10] and nanowires [11].

*Corresponding author: Anita R. Warrier
E-mail: anitawarrier2@gmail.com

Paper received: 29.01.2025.
Paper corrected: 19.02.2025.
Paper accepted: 23.02.2025.

The synthesis methodology and conditions determine the crystallinity, purity, and morphology of SnO_2 nanostructures. SnO_2 nanoparticles can be synthesized by various methods such as chemical precipitation [12], microwave [13], gel combustion route, sol-gel [14,15], solvothermal [16], hydrothermal [17], sonochemical, mechano-chemicaland solid-state method.

Srivastava et al have synthesized tetragonal $SnO_2$with a crystallite size of 10 nm by thermal treatment at 600°C for 3 h using the microwave method (2.45 GHz) with power up to 1 KW for a duration of 260s, which is energy efficient and obtained SnO_2 phase which is non-agglomerated [18]. SatishKumar et al have synthesized tetragonal SnO_2nanoparticles of size 29 nm using the microwave method (2.45 GHz) with power up to 900 W and irradiated for 15 min [19]. Parthibavarman et al obtained SnO_2nanoparticles of size 25-30 nm, with tetragonal rutile structure using the microwave method (2.45 GHz) with power up to 900 W and irradiated for 10 min [20].

Aziz et al have reported on the synthesis of SnO_2 nanoparticles of uniform crystallite size of 22 nm -31 nm by sol-gel method using PEG. The mean size of the particles increases with an increase in calcination temperature and the surface area of the nanomaterials decreases upon thermal treatment [21]. Nasrin Talebian et al have reported on the synthesis of flower-shaped SnO_2

nanoparticles by hydrothermal method with enhanced photodegradation efficiency [22].

R.Al-Gaashani etal have reported on the synthesis of SnO_2nanoparticles of various sizes and morphology by thermal decomposition of $SnCl_2.2H_2O$ at differenttemperatures and times. The crystallite size of the SnO_2 nanoparticles with tetragonal structure increases from 25 nm to 53 nm, an optical band gap of 3.9 eV to 3.7 eVwith the increase in the decomposition temperature from 400˚C and 900˚Cand an increase in preparation time from 20 min-60 min. The change in temperature leads to interesting morphologies like rabbit tail-like, grass-like, hexagonal, and brain-like structures [23].

SnO_2 nanostructures are one of the most favored materials for gas sensors [24-25], transparent electrodes, liquid crystal displays, lithium-ion batteries, photosensors, antistatic coating, transistors, electrode materials, catalysts [26], optoelectronic devices [27], catalyst supports, antireflective coatings, solar cells [28], and electrochromic devices.SnO_2 is highly favored, as it is non-toxic and doesn't show any health effects as the human body doesn't absorb the nanoparticles even when inhaled. Also,SnO_2 shows dual valency and can attain more oxidation states preferably 2^+ or 4^+ [29], which helps SnO_2 to show different surface properties. Especially, SnO_2 has highly acidic, basic, oxidizing, and reducing surface properties and is treated as a superacid. Lam et al have reported that SnO_2 promotes catalytic reactions due to the presence of a large number of strong acid sites. These properties make them highly suitable for catalytic applications.

SnO_2hashigh electrical conductance, transparency to visible light, outstanding photoelectric properties,and strong surface interaction with toxic gas molecules. Due to these properties,when SnO_{2is} coated in gas–sensing devices, the measurement of the electrical conductivity determines the concentration of inflammable/toxic gases (H_2, CO, CH_4). Further,the gas sensitivity of nanocrystalline SnO_2(< 10 nm) sensors is much enhanceddue toan increase in active surface sites which promotes adsorption/desorption. SnO_2nanomaterialsin various morphologies show promise as a catalyst for CO oxidation, methanol and ethanol electrooxidation, H_2 evolution, and hydrogenation of esters.

Agrahari et al have reported on the rutile (tetragonal) SnO_2 nanoparticles by co-precipitation method. SnO_2 nanoparticles show photoluminescence emission in blue (480 nm-484 nm) and green regions (520 nm -527 nm), photoconductivity, and room temperature ferromagnetism which makes them suitable as dilute magnetic semiconductors[30].Tran et al have reported on the SnO_2 nanoparticles as a cathode base layer using spin coating method with a band gap of ~ 3.94 eV [31]. Liu et al have reported that quantum-sizeSnO_2 nanoparticles can act as electron transportation layer material in CdSe-based QD-LEDs [32]. Oxygen vacancies, metal ion interstitials, or dangling bonds contribute to the luminescence of SnO_2 nanoparticles, which further makes it a suitable material for nanoscalelight-emitting devices. Luminescence and defect concentration change with the shape and size of the nanoparticles. Vasanthi et alhave reported on the synthesis of pure and Cd^{2+} doped (10 mol% and 20 mol%) SnO_2 nanoparticles by microwave-assisted sol-gel combustion method. The emission band intensity is higher for Cd-dopedSnO_2 nanoparticles (10 mol% Cd) thanforundopedSnO_2 nanoparticles followed by Cd-dopedSnO_2 nanoparticles (20 mol% Cd). Cd doped (10 mol%)SnO_2 nanoparticles show higher emission intensity when compared to that of undopedSnO_2 nanoparticles and Cd doped (20 mol%)SnO_2 nanoparticles, which is due to the increased concentration of surface oxygen vacancies as well as singly ionized vacancies due to its reduced size [33].

In this work, we report on the synthesis of SnO_2 nanoparticles by thermal decomposition method and study the impact of decomposition temperature on structure, microstrain, morphology, Raman active and IR active modes, optical band gap, and photoluminescence. The nanoparticles were characterized using X-ray diffraction (XRD), Fourier Transform Infrared Spectroscopy (FT-IR), Raman Spectroscopy, Scanning Electron Microscopy (SEM), UV-Vis spectroscopy, and photo luminescence spectroscopy. The XRD spectrum was recorded using PANalyticalX'Pert Pro diffractometer using Cu–Kα radiation (λ = 1.5418 Å). The phases present in the synthesized nanoparticleswere identified usingthe JCPDS (Joint Committee of the Powder Diffraction Standard) database files. Microstrain and crystallite size of the synthesized samples were calculated from the XRD pattern with the help of William–Hall's equation. The functional groups present in the sample were identified usinga Fourier-transform infrared spectrometer (Thermo Nicolet, Model number: 6700)in the range of 400–4000 $cm^{-1}$with the KBR pellet method.The opticalband gapwas calculated from the wavelength-dependent absorption coefficient measured using a UV-Vis spectrophotometer (Agilent, Cary 60) in the range of 300 nm to 800 nm.SEM images were obtained using Scanning Electron Microscopy (Model number: S-3400N, Hitachi) and the Raman

spectrum was recorded usingan Invia Reflex Raman Microscope with Spectrometer (Renishaw Metrological Systems UK).Photoluminescence spectrum is obtained using a Spectrofluorometer (Model: Fluorolog- FL3-11) with excitation at a wavelength of 250 nm using anXenon lamp, in the emission range of 250 nm-500 nm.

2. SYNTHESIS OF TIN OXIDE NANOPARTICLES BY THERMAL DECOMPOSITION METHOD

1.15 g of tin (II) chloride dihydrate was weighed in a silica crucible and then heated in a muffle furnace. In the first step of the reaction, as we increase the temperature from 80˚C to 160˚C, tin (II) chloride dihydrate decomposes to produce $Sn_4(OH)_6Cl_2$, HCl, and H_2O.

$$4SnCl_2.2H_2O \xrightarrow{80-160^{\circ}C} Sn_4(OH)_6Cl_2(s) + 6HCl\ (g) \uparrow + 2H_2O(g) \uparrow \quad (1)$$

In the second step (temperature range 160–250˚C), part of the $Sn_4(OH)_6Cl_2$ will decompose to form Sn (liquid) and $SnOCl_2$, then Sn will react partially with HCl to give a mixture of Sn and $SnCl_2$.

$$Sn_4(OH_6)Cl_2 \xrightarrow{160-250^{\circ}C} 3Sn + SnOCl_2(s) + 3H_2(g) \uparrow + 2.5\ O_2(g) \uparrow \quad (2)$$

In the third stage of the reaction at 400˚C, the following reactions lead to the formation of SnO_2.

$$SnOCl_2.0.5O_2(g) \xrightarrow{20\ min\ at \geq 400^{\circ}C} SnO_2(s) + Cl_2(g) \uparrow \quad (3)$$

(or)

$$SnOCl_2(s) \xrightarrow{20\ min\ at \geq 400^{\circ}C} SnOCl(s) + Cl(g) \uparrow \quad (4)$$

$$2SnOCl(s) \xrightarrow{20\ min\ at \geq 400^{\circ}C} SnO_2(s) + SnCl_2(g) \uparrow \quad (5)$$

$$Sn(l) + O_2 \xrightarrow{20\ min\ at \geq 400^{\circ}C} SnO_2 \quad (6)$$

Upon completion of the reaction, a grey color fine powder was obtained. Samples were prepared at decomposition temperatures300˚C, 400˚C, 500˚C and 600˚Cfor a reaction time of 20 minutes.

3 RESULTS AND DISCUSSION

According to group theory, the normal lattice vibration calculated at the Γ point of the Brillouin zone [34,35] for rutileSnO_2 nanoparticles belonging to the space group of D_{4h} is given in equation 7.

$$\Gamma = 1A_{1g} + 1A_{2g} + 1A_{2u} + 1B_{1g} + 1B_{2g} + 2B_{1u} + 1E_{1g} + 3E_u) \quad (7)$$

Where

A_{1g}, B_{1g}, B_{2g}, and E_{1g} are considered to be Raman active modes, A_{2u} and E_u are symmetrical infrared active modes and symmetrical A_{2g} and $B_{1u}$are considered to be optically inactive Raman modes of SnO_2 nanoparticles.

The Raman spectrum for SnO_2 nanoparticles synthesized at thermal decomposition temperatures of 300˚C and 400˚C is depicted in Fig.1(a). These samples showRaman'sshift at 157 cm^{-1}, 163 cm^{-1}, 184 cm^{-1}, 194 cm^{-1} which is due to the presence of unreacted $SnCl_2$[36]. There is no peak corresponding to the SnO_2 phase for decomposition temperature at 300˚C. At 400˚C, the Raman shift at 106 cm^{-1} and 214 cm^{-1} corresponds to the B_{1g} and A_{1g}modesof SnO [37-39].

Bulk SnO_2 nanoparticles have active Raman modesE_{1g}, A_{1g}, B_{2g}at 474.0 cm^{-1}, 632.0 cm^{-1} and 774.0 cm^{-1} respectively. Figure 1(b) shows the Raman spectra of samples synthesized at 500˚C and 600˚C. The three fundamental vibrational modes of rutileSnO_2(E_g(478 cm^{-1}), A_{1g}(634 cm^{-1}) and B_{2g} (772 cm^{-1})) are observable for samples decomposed at 500˚C and 600˚C. The red-shift in Raman modes in comparison to bulk SnO_2 is due to quantum confinement and change in defect concentration, which distorts the Raman scattering profiles. The weak Raman shift at 681 cm^{-1} is due to the interior phonon mode (A_{2g}) [30]. Thus, pure-phaseSnO_2 nanoparticles are formed only when the thermal decomposition temperature is ≥500˚C.The broad, low-frequency peaks at 249 cm^{-1} and 305 cm^{-1}which are rarely seen in bulk are prominent in SnO_2 nanoparticles (Figure 1b) [40]. These inactive modes($E_{u(TO)}$ mode (TO- mode of transverse optical phonons)) become active in nanoparticles due to the splitting down of the symmetry restriction.

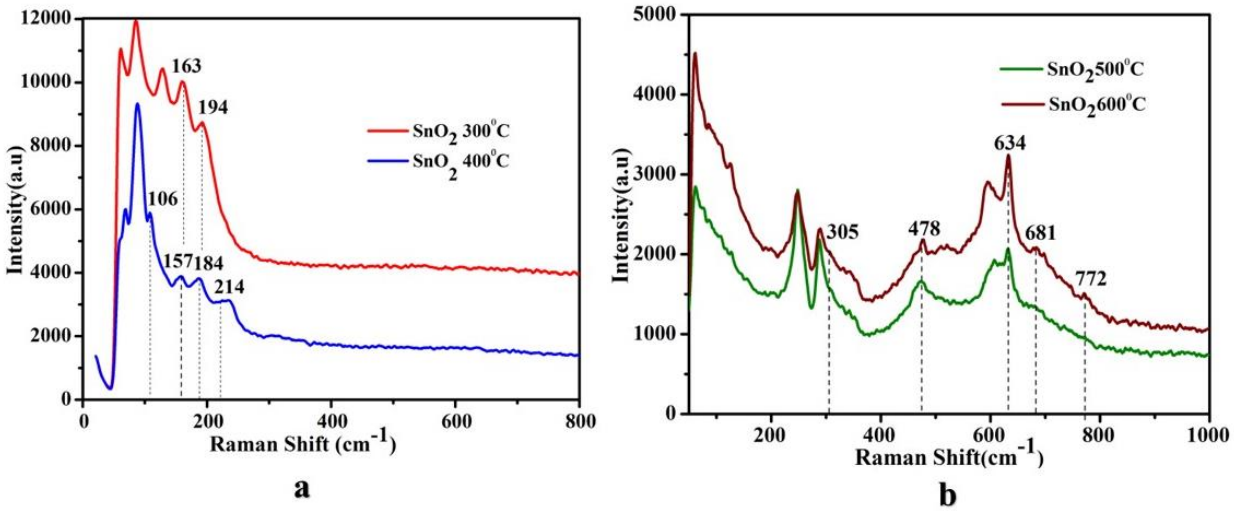

Figure 1. (a) Raman spectrum for SnO_2 nanoparticles synthesized at thermal decomposition temperatures 300˚C and 400˚C (b) 500˚C and 600˚C.

Fig.2 (a) shows the FTIR spectrum of SnO_2 nanoparticles synthesized at 600˚C. The peaksseen at 491 cm^{-1} and 626 cm^{-1} are due to terminal Sn-O mode and O-Sn-O bond vibration [41-43]. The peak at 3444 cm^{-1} comes from the stretching mode vibrations of the O-H bond [44]. The spectrum does not show the formation of any other impurity phases.

Fig.2 (b) shows the XRD pattern of SnO_2 nanoparticles prepared by thermal decomposition at different temperatures (300˚C, 400˚C, 500˚C and 600˚C) for a fixed duration (20 minutes). The synthesized SnO_2 nanoparticles represent the rutile (tetragonal) phase of $SnO_2$with orientation along [110], [101], [200], [211], [220], [310], [112], [301], [202], [321] crystal planes. The increase in thermal decomposition temperature does not change the crystal structure of SnO_2 and crystal plane orientation [45]. The relative intensities of the peaks increase for SnO_2samplessynthesized at higher temperatures. For SnO_2 samples prepared at the temperature of 300˚C, the peaks corresponding to SnO_2 are weak and show the presence of impurity phases such as $Sn_4(OH)_6Cl_2$ and $SnCl_2$. These impurity phases diminish upon an increase in decomposition temperature and the SnO_2 peaks become dominant.

The crystallite size (D) was estimated from Scherrer's equation 8.

$$D = \left(\frac{K\lambda}{\beta Cos\theta}\right) \qquad (8)$$

in which (λ) is the wavelength (λ=1.54056 Å)

K is the Scherrer constant = (0.94)

β is the full width at half maximum (FWHM in radians)

θ is the diffraction angle of Bragg, and

D is the particle size (nm).

The average crystallite size (~15 nm) of the SnO_2 nanoparticles has been estimated by applying the Scherrer formula for samples treated at 400˚C and 500˚C considering [211] plane. However, the crystallite size is reduced to ~ 9 nm for a decomposition temperature of 600˚C along the [211] plane. Table 1 below shows the crystallite size calculated for the synthesized samples.

Table 1

Thermal decomposition temperature(°C)	2θ (degrees)	Plane	Crystallite size (nm)
400	51.74	[211]	15.53
500	51.74	[211]	15.2
600	51.74	[211]	9

Table 1 shows the crystallite size calculated for the synthesized samples.

The crystallite size calculated from all the planes is given in Tables 2, 3, and 4.

Table 2

Thermal decomposition temperature 600°C		
2θ (degrees)	Plane	Crystallite size (nm)
26.63	[110]	13.7
33.94	[101]	12.77
37.95	[200]	11.98
51.74	[211]	9
54.78	[220]	11.87
61.93	[310]	12.86
64.63	[112]	14.77
65.9	[301]	11.91
71.3	[202]	14.66

Table 2 shows the crystallite size calculated from all the planes of SnO_2 nanoparticles synthesized at 600˚C

Table 3

Thermal decomposition temperature 500˚C		
2θ (degrees)	Plane	Crystallite size (nm)
26.63	[110]	14.6
33.94	[101]	15.1
37.95	[200]	14.8
51.74	[211]	15
54.78	[220]	15.1
61.93	[310]	15.8
64.63	[112]	16.9
65.9	[301]	14.3
71.3	[202]	17.4

Table 3 shows the crystallite size calculated from all the planes of SnO_2 nanoparticles synthesized at 500˚C.

Table 4

Thermal decomposition temperature 400˚C		
2θ (degrees)	Plane	Crystallite size (nm)
26.63	[110]	14.9
33.94	[101]	14.2
37.95	[200]	12.6
51.74	[211]	15
54.78	[220]	15
61.93	[310]	14.43
64.63	[112]	15.76
65.9	[301]	11.88
71.3	[202]	17.76

Table 4 shows the crystallite size calculated from all the planes of SnO_2 nanoparticles synthesized at 400˚C.

As the calcination temperature increases, the diffraction peaks become sharper and more intense, indicating particle growth and improved crystal quality. No significant changes were observed in the positions and intensities of the peaks for the samples synthesized at lower calcination temperatures. The sample synthesized at 600 ^{0}C shows a reduction in the intensity of the [220] peak, due to the greater number of lattice sites and disorders [46]. Moreover, the vacancies can aggregate and form vacancy clusters at the interface, resulting in a localized interfacial state for the samples synthesized at 600 ^{0}C and higher. The observed ratio of peak intensities of the SnO_2 nanoparticles synthesized at 600^{0}C does not match the standard reference data [47] hence the critical temperature for formation of SnO_2 crystals is 500^{0}C. This can be due to the disrupted packing caused by oxygen vacancies in certain lattice planes of SnO_2 nanoparticles synthesized at 600 ^{0}C [48]. Vladimir has also reported that annealing at temperatures greater than 550 ^{0}C leads to the formation of SnO_2 films [49]. Fig.3 shows the particle size distribution for the SnO_2 nanoparticles synthesized at temperatures of 400 ^{0}C, 500˚C and 600 ^{0}C.

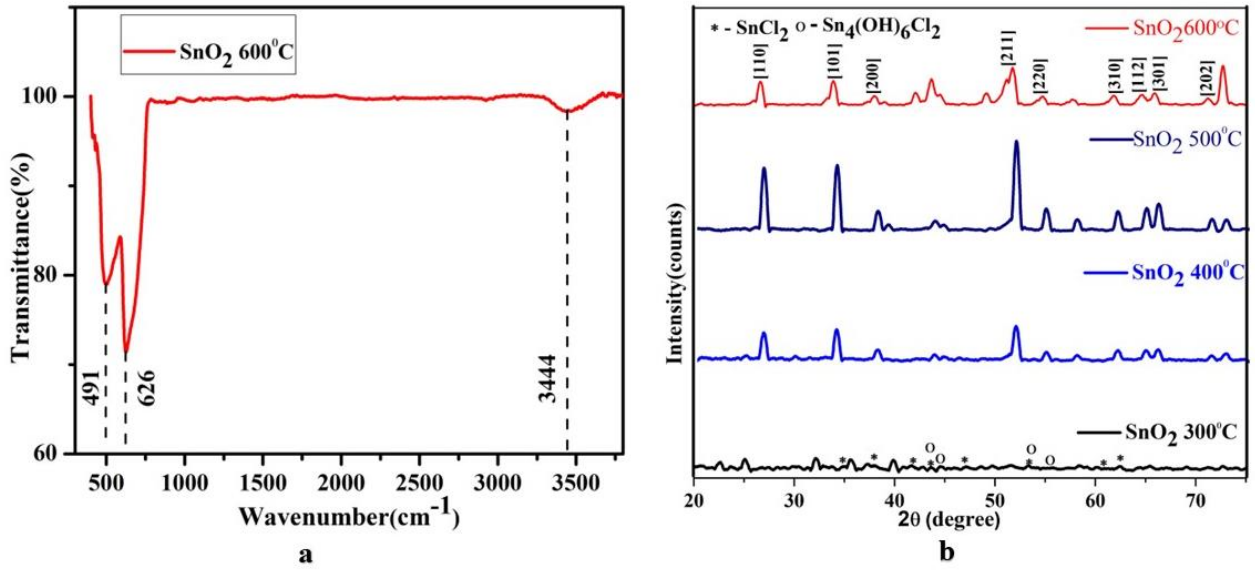

Figure 2. (a) FTIR spectrum of SnO_2 nanoparticles synthesized at 600 ^{0}C (b) XRD pattern of SnO_2 nanoparticles treated at 300 ^{0}C, 400 ^{0}C, 500 ^{0}C and 600 ^{0}C

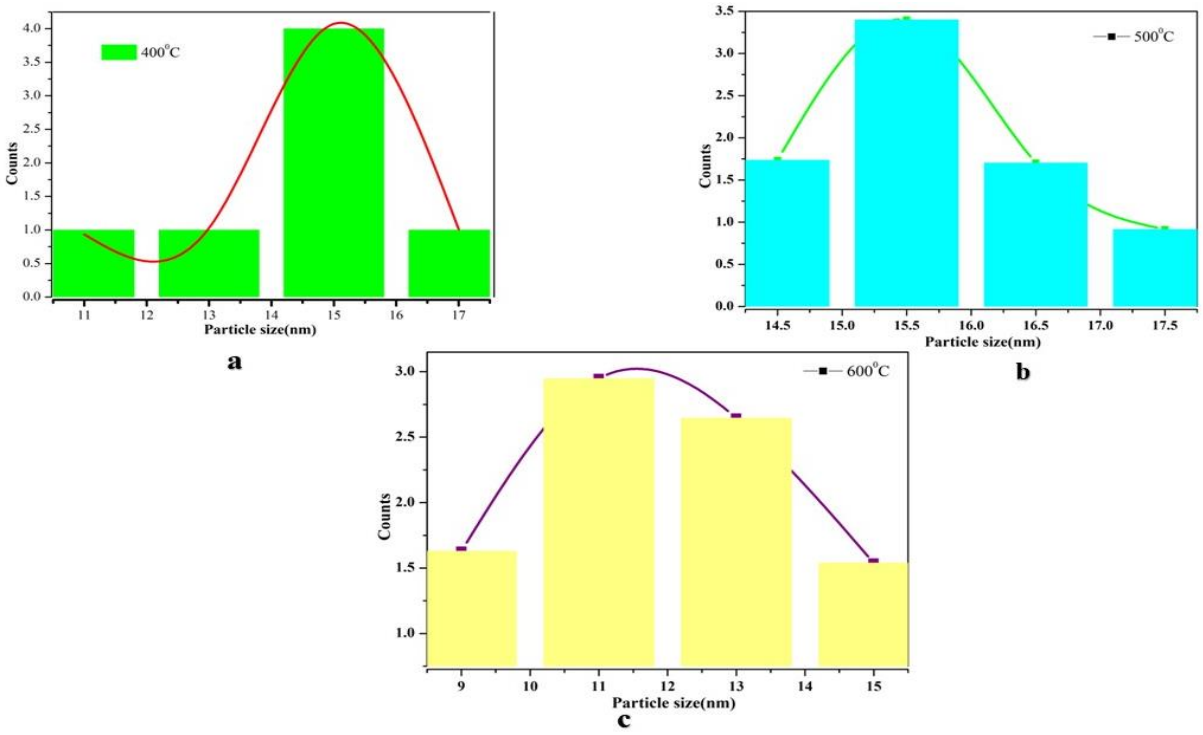

Figure 3. The particle size distribution for the SnO_2 nanoparticles synthesized at temperatures of 400 ^{0}C, 500 ^{0}C and 600 ^{0}C

The strain induced in the nanoparticles is directly proportional to the full width at half maximumand is due to the crystal defect and distortion calculated using the relation [50],

$$\varepsilon = \frac{\beta_{hkl}}{4tan\theta} \quad (9)$$

Peak broadening is due to the contribution of the particle size and strain which are not dependent on each other. The particle size and strain showa Cauchy-like profile and the peak width is given as the sum of equations 8 and 9,

$$\beta_{hkl} = \frac{K\lambda}{Dcos\theta} + 4\varepsilon tan\theta \quad (10)$$

By rearranging the above equation

$$\beta_{hkl}\, cos\theta = \frac{K\lambda}{D} + 4\varepsilon\, sin\theta \quad (11)$$

The above equations are the Williamson-Hall equation. The graph was drawn between 4sinθ(in x axis) and β_{hkl}cosθ(in y-axis) for the synthesized SnO_2 nanoparticles with a rutile (tetragonal) phase. The crystallite size of the SnO_2 nanoparticle was determined from the intercept and strain values from the slope of the graphconsidering all the XRD peaks for the samples synthesized by thermal decomposition at 400˚C, 500˚C, and 600˚C. Equation11shows the union deformation model (UDM), in which the strain was considered uniform in all crystallographic directions, taking into account the isotropic nature of the crystal, in which the material's properties are independent of the direction in which the measurement was carried out.SnO_2 nanoparticles synthesized at 600^{o}C exhibit a positive lattice strain of + 0.35731 x 10^{-3} indicating tensile strain whereas a negative lattice strain of -0.4966 x 10^{-3} and -0.90158 x 10^{-3} exhibits compressive strain for nanoparticles synthesized at 400^{o}C and 500^{o}C.Fig.4(a),(b),and (c) shows the microstrain and crystallite size determination for SnO_2 nanoparticles synthesized at temperatures of 400˚C, 500˚C, and 600˚C assuming uniform deformation model. Fig.4(a) and (b) show a negative strain for SnO_2 nanoparticles synthesized at 400˚C and 500˚C. This induced compressive strain was due to the lattice shrinkage which was seen in the lattice parameter calculations [51]. The sample synthesized at 600˚C shows a positive signal of the micro-strain due to the lattice expansion [52].

Lattice strain estimates the distribution of lattice constants created from crystal imperfections like lattice dislocation [53]. As the crystallite size reduces for the sample synthesized at 600^{0}C, increased surface atoms exhibit relaxation due to the reduced coordination and bonding, leading to lattice expansion and enhanced strain[54]. Oxygen vacancies can also create local lattice distortions causing an increase in strain and lattice expansion. This lattice expansion may also occur due to the removal of oxygen atoms leading to a reduction in the coordination of tin atoms, thereby expanding the lattice to reconfigure for the bonding changes seen in SnO_2 nanoparticles synthesized at 600˚C.

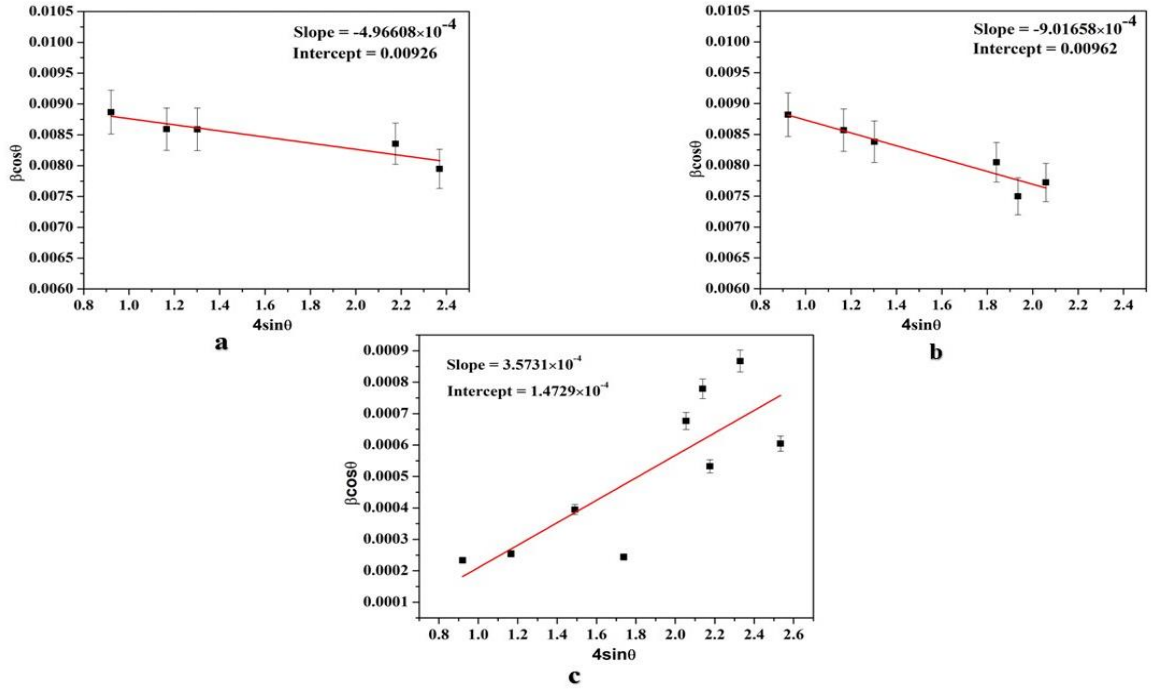

Figure 4. (a), (b), (c) The microstrain and crystallite size determination for SnO_2 nanoparticles synthesized at temperatures of 400˚C, 500˚C and 600˚C assuming union deformation model.

Table 5. Crystallite size and microstrain from William Hall equation D (nm) using the Union deformation model

S.No	Sample calcination temperature in °C	Crystallite size from Scherrer equation D (nm)	Crystallite size from William Hall equation D (nm) using Union deformation model (UDM)	Microstrain (Ɛ)x10-3
1	400	15.53	15.16	-0.496608
2	500	15.2	14.82	-0.901658
3	600	9	9.85	0.35731

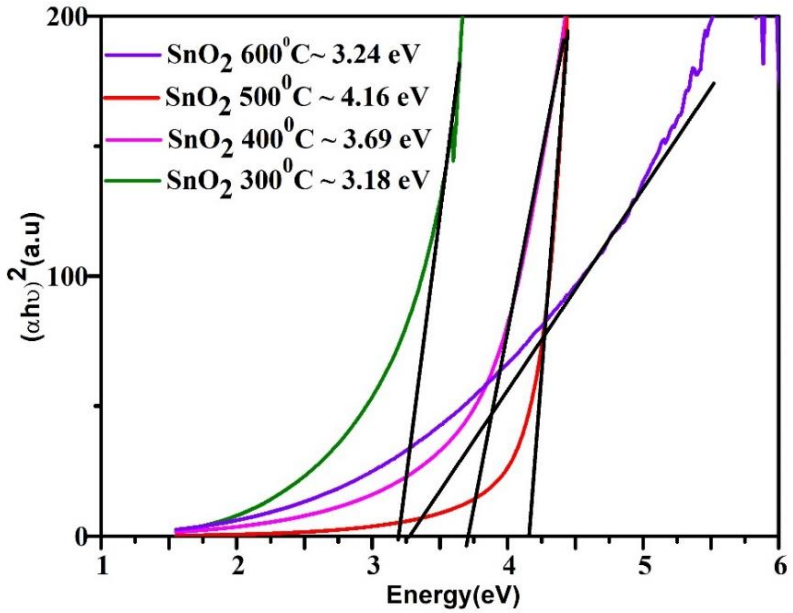

Figure 5. The Tauc plot of SnO_2 at different thermal decomposition temperatures 300˚C, 400˚C, 500˚C and 600˚C

Fig.5 shows the Tauc plot of SnO_2 at different thermal decomposition temperatures obtained from the optical absorption spectrum. The band gap energy calculated for SnO_2 nanoparticles synthesized at 300˚C, 400˚C, 500˚C and 600˚Cis 3.18 eV, 3.72 eV, 4.16 eV, and 3.64eV respectively [55-61,45]. But for SnO_2 nanoparticles synthesized at 600˚C there is a decrease in the band gap anda decrease in the defect absorption which could be due to the phases of SnO [62].

Fig.6 shows the morphology of SnO_2 nanoparticles synthesized at 600˚C. It can be observed that SnO_2 nanoparticles are agglomerated which depends on the size of the particles. The size of the SnO_2 nanoparticles is estimated to be 9 nm from XRD. As the size of the particles increases in the nanoscale, the particles also get agglomerated.

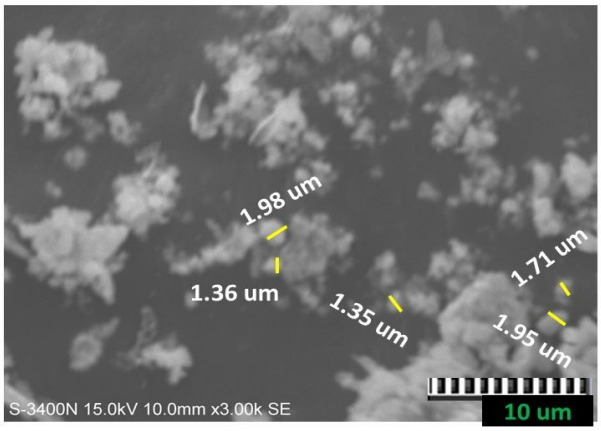

a)

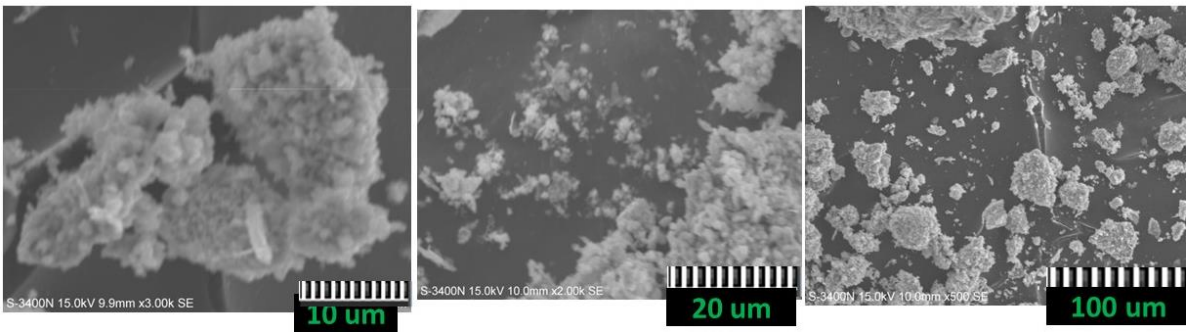

(b)

Figure 6. (a), (b) SEM images showing the structure of SnO_2 nanoparticles (9 nm) calcinated at 600˚C for 20 min

Figure 7 shows Photoluminescence spectrum of SnO_2 nanoparticles synthesized at 300˚C, 400˚C, 500˚C and 600˚C.Visible emission peaks seen in the photoluminescence spectra are due to intrinsic defects such as oxygen vacancies, Sn interstitials, and Sn vacancies which may occur during the synthesis of the sample. The peaks of varying intensities are found at 330,352, 369,397,420,432, 450,and 467 nm. The emission peak at 330 nm is due to the direct recombination of electrons from the Sn_{4p} conduction band to the hole in the O_{2p} valance band. The peak at 352 nm is due to the near band edge emission of the SnO_2 nanoparticles. The peak at 369 nm is generally assigned to the band to acceptor transition and is related to the impurity or defect concentration. The emission peak at 397 nm can be attributed to structural defects or luminescent centers, such as nanocrystals and defects in SnO_2 nanoparticles.

The emission peaksat 420 and 467 nm correspond to violet and blue colors. Blue emission arises from the surface states such as oxygen vacancy. Normally the oxygen vacancies exist in three charge states of V_o^o, $V_o^{+,}$ and V_o^{++}[63,64]. $V_o^o$is considered to be a shallow donor and it is seen that oxygen vacancies will be present in their paramagnetic V_o^+ state in flat band conditions. The peak at 432 nm emission is due to the Sn interstitials. The peak seen at 450 nm,and 467 nm is due to the oxygen vacancy with two trapped electrons, V_o^{++} which is due to the recombination of the surface trapped hole with an electron present in the deep trap (V_o^+). Moreover, oxygen vacancies are predominantly the most common defects that act as radiative centers in luminescence processes for polycrystalline and nanocrystalline oxides.

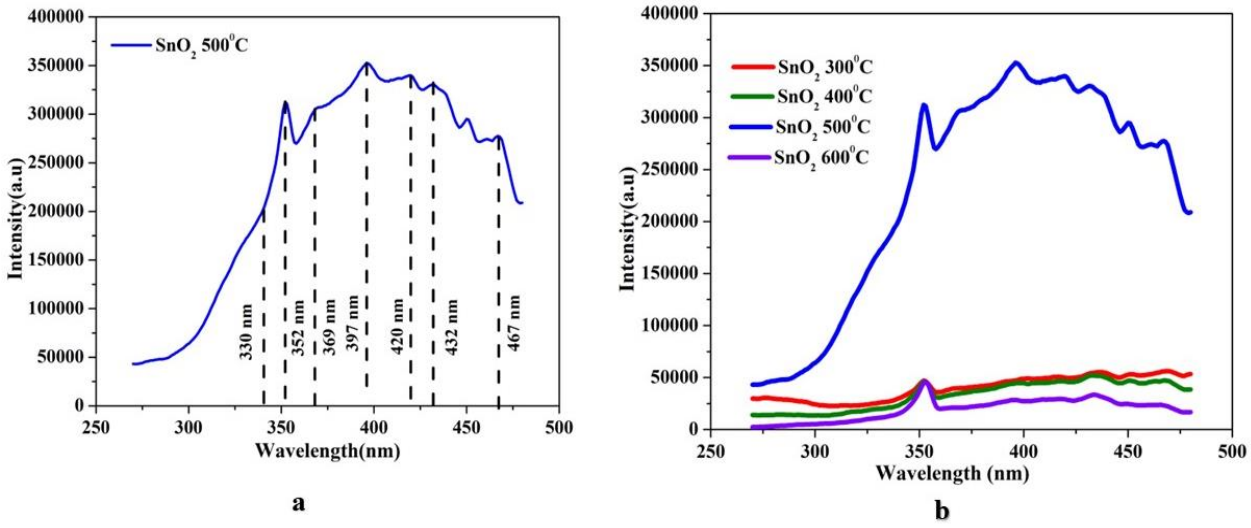

Figure 7. Photoluminescence spectra of SnO_2 nanoparticles

4. CONCLUSION

Rutile phase SnO_2 nanoparticles with a size of ~ 9 nm were synthesized by the thermal decomposition method at different temperatures. At temperatures below500˚Cthe particles acquire a negative strain due to the lattice shrinkage and above 500˚Cthe strain is positive due to the lattice expansion. The SnO_2 nanoparticles synthesized at 500˚C are highly transparent and Raman active with a band gap of ~ 4.16 eV. At 500˚C,the emission is broad and intense (5 x10^5counts) at 450 nm which is attributed to the high crystallinity, low lattice strain, and increase in oxygen vacancy.

Acknowledgment

We acknowledge the Academy of Maritime Education and Training for providing us with the startup grant to carry out this work.

REFERENCES

[1] G.H.Patel, S.H.Chaki, R.M.Kannaujiya, Z.R. Parekh, A.B.Hirpara (2021) Sol-gel synthesis and thermal characterization of SnO_2 nanoparticles. Physica B: Condensed Matter, 613,412987 https://doi.org/10.1016/j.physb.2021.412987

[2] S.G. Onkar, F.C.Raghuwanshi, D.R.Patil, T. Krishnakumar (2020) Synthesis, characterization and gas sensing study of SnO_2 thick film sensor towards H_2S, NH_3, LPG and CO_2.Materials Today Proceedings, 23,190–201 https://doi.org/10.1016/j.matpr.2020.02.017

[3] S. Lopez-Moreno, A.H.Romero, J. Mejia-Lopez, A.Munoz (2016) First-Principles Study of Pressure-Induced Structural Phase Transitions in MnF_2.Physical Chemistry Chemical Physics,18*(48),* 33250−33263 https://doi.org/10.1039/C6CP05467F

[4] I. Erdem, H. H. Kart, T.Cagin (2014) High Pressure Phase Transitions in SnO_2 Polymorphs by First-Principles Calculations. Journal of Alloys and Compounds, 587**,** 638−645 https://doi.org/10.1016/j.jallcom.2013.10.238

[5] D.Mohanta, M. Ahmaruzzaman (2016) Tin Oxide Nanostructured Materials: An Overview of Recent Developments in Synthesis, Modifications and Potential Applications. RSC Advances, 6(112),110996−111015, https://doi.org/10.1039/C6RA21444D

[6] J. Chao, D. Zhang, S. Xing, Y. Chen, W.Shen (2018) Controllable Assembly of Tin Oxide Thin Films with Efficient Photoconductive Activity. Materials Letters, 229**,** 244−247, https://doi.org/10.1016/j.matlet.2018.07.027

[7] Q. Wang, N. Yao, D. An, Y. Li, Y.Zou (2016) Enhanced gas sensing properties of hierarchical SnO_2nanoflower assembled from nanorods via a one-pot template-free hydrothermal method. Ceramics International,42,15889–15896, https://doi.org/10.1016/j.ceramint.2016.07.062

[8] J. Hu, X. Li, X. Wang, Y. Li, Q. Li (2018) Hierarchical aloe-like SnO_2nanoflowers and their gas sensing properties.Journal of Materials Research, 33**,** 1433–1441, https://doi.org/10.1557/jmr.2018.94

[9] Y.Zeng,Y. Wang, L.Qiao, Y. Bing,B.Zou (2016) Synthesis and the improved sensing properties of hierarchical SnO_2 hollow nanosheets with mesoporous and multilayered interiors. Sensors and Actuators B:Chemical**,** 222,354–361,https://doi.org/10.1016/j.snb.2015.08.068

[10] G. Li, Z. Cheng, Q. Xiang, L. Yan, X. Wang (2019) Bimetal PdAu decorated SnO_2 nanosheets based gas sensor with temperature-dependent dual selectivityfor detecting formaldehyde and acetone. Sensorsand Actuators B: Chemical,283,*590–601*, https://doi.org/10.1016/j.snb.2018.09.117

[11] Z. U.Abideen, J. H. Kim, S. S. Kim (2017) Optimization of metal nanoparticle amount on SnO_2 nanowires to achieve superior gas sensing properties. Sensors and Actuators B: Chemical, 238,374–380, https://doi.org/10.1016/j.snb.2016.07.054

[12] D. Varshney, K. Verma (2013) Effect of stirring time on size and dielectric properties of SnO_2 nanoparticles prepared by co-precipitation method. Journal of Molecular Structure, 1034,216-222, https://doi.org/10.1016/j.molstruc.2012.10.049

[13] M.Akram, A. T.Saleh, W. A. Wan Ibrahim, A. S.Awan, R.Hussain (2016) Continuous microwave flow synthesis (CMFS) of nano-sized tin oxide: effect of precursor concentration. Ceramics International, 42, 8613–8619 https://doi.org/10.1016/j.ceramint.2016.02.092

[14] A. S.Ahmed, A.Azam, M.Shafeeq M, M.Chaman, S.Tabassum (2012) Temperature-dependent structural and optical properties of tin oxide nanoparticles. Journal of Physics and Chemistry of Solids, 73,943–947 https://doi.org/10.1016/j.jpcs.2012.02.030

[15] A. Lemarchand, F.Remondiere, J.Jouin, P. Thomas, O. Masson (2020) Crystallization pathway of size-controlled SnO_2 nanoparticles synthesized via a nonaqueoussol-gel route. Crystal Growth Design,20,1110–1118 https://doi.org/10.1021/acs.cgd.9b01428

[16] S. Das, S.Kar, S.Chaudhuri (2006) Optical properties of SnO_2 nanoparticles and nanorod synthesized by solvothermal process. Journal of Applied Physics, 99,114–303 https://doi.org/10.1063/1.2200449

[17] M.A.M.Akhir,K. Mohamed, Lee. H.L, S. A.Rezan (2016) Synthesis of tin oxide nanostructures using hydrothermal method and optimization of its crystal size by using statistical design of experiment. Procedia Chemistry, 19,993–998 https://doi.org/10.1016/j.proche.2016.03.148

[18] A. Srivastava, S.T.Lakshmikumar, A.K. Srivastava, Rashmi, K. Jain (2007) Gas sensing properties of nanocrystallineSnO_2 prepared in solvent media using a microwave-assisted technique.Sensors and Actuators B:Chemical, 126,583–7 https://doi.org/10.1016/j.snb.2007.04.006

[19] M.Sathishkumar, S.Geethalakshmi (2019) Enhanced photocatalytic and antibacterial activity of Cu:SnO_2 nanoparticles synthesized by microwave assisted method. Materials Today: Proceedings, 20,54-63, https://doi.org/10.1016/j.matpr.2019.08.246

[20] M.Parthibavarman, K.Vallalperuman, S. Sathishkumar, M. Durairaj & K.Thavamani (2013) A novel microwave synthesis of nanocrystalline SnO_2 and its structural optical and dielectric properties. Journal of Materials Science: Materials in Electronics,25(2),730–735, https://doi.org/10.1007/s10854-013-1637-9

[21] M. Aziz, S. S. Abbas, W. R. W.Baharom, W. Z. W. Mahmud (2012) Structure of SnO_2 nanoparticles by sol-gel method. Materials Letters, 74*, 62–64,* https://doi.org/10.1016/j.matlet.2012.01.073

[22] N.Talebian, F.Jafarinezhad (2013)Morphology-controlled synthesis of SnO_2 nanostructures using hydrothermal method and their photocatalytic applications. Ceramics International, 39(7), 8311–8317 https://doi.org/10.1016/j.ceramint.2013.03.101

[23] R.A.Gaashani, S.Radiman, N.Tabet, A.R.Daud (2012) Optical properties of SnO_2 nanostructures prepared via one-step thermal decomposition of tin (II) chloride dihydrate. Materials Science and Engineering: B*,* 177(6), 462–470 https://doi.org/10.1016/j.mseb.2012.02.006

[24] L. Song, B. Zhao, X.Ju, L.Liu,Y. Gong (2020) Comparative study of methanol gas sensing performance for SnO_2 nanostructures by changing their morphology. Materials Science in Semiconductor Processing*,* 111, 104986 https://doi.org/10.1016/j.mssp.2020.104986

[25] E. T. H Tan, G. W. Ho, A. S. W Wong, S. Kawi, A. T. S Wee (2008) Gas sensing properties of tin oxide nanostructures synthesized via a solid-state reaction method. Nanotechnology,19, 255706 https://doi.org/10.1088/0957-4484/19/25/255706

[26] A. Liu, M. Zhu, B. Dai (2019) A novel high-performance SnO_2 catalyst for oxidative desulfurization under mild conditions. Applied Catalysis A: General, 583, 117134 https://doi.org/10.1016/j.apcata.2019.117134

[27] D. H. Kim, S. Y. Kim, S. W.Han,Y. K. Cho, M.-G.Jeong (2015) The catalytic stability of TiO_2-shell/Ni-core catalysts for CO_2 reforming of CH_4.Applied Catalysis A: General,495, 184–191 https://doi.org/10.1016/j.apcata.2015.02.015

[28] Y. Chen, Q.Meng, L. Zhang, C. Han, H.Gao (2019) SnO_2-based electron transporting layer materials for perovskite solar cells: a review of recent progress. Journal of Energy Chemistry, 35,144–167, https://doi.org/10.1016/j.jechem.2018.11.011

[29] S.Tazikeh, A.Akbari, A.Talebi, E.Talebi (2014) Synthesis and characterization of tin oxide nanoparticles via the Co-precipitation method. Materials Science-Poland, 32(1), 98–101, https://doi.org/10.2478/s13536-013-0164-y

[30] V.Agrahari, M. C.Mathpal, M. Kumar,A. Agarwal (2015) Investigations of optoelectronic properties in DMSSnO_2nanoparticles.Journal of Alloys and Compounds*,* 622*,*48–53 https://doi.org/10.1016/j.jallcom.2014.10.009

[31] V. H. Tran, R.B.Ambade, S.B.Ambade, S.H. Lee, I. H. Lee (2017) Low-Temperature Solution-Processed SnO_2 Nanoparticles as a Cathode Buffer Layer for Inverted Organic Solar Cells. ACS Applied Materials & Interfaces, 9(2),1645–1653 https://doi.org/10.1021/acsami.6b10857

[32] Y. Liu, S. Wei, G. Wang, J. Tong, J. Li (2020) Quantum Sized SnO_2 Nanoparticles with Up-Shifted Conduction Band: A Promising Electron Transportation Material for Quantum Dot Light-Emitting Diode. Langmuir, 36 (23),6605–6609 https://doi.org/10.1021/acs.langmuir.0c00107

[33] V.Vasanthi, M.Kottaisamy, K.Anitha, V. Ramakrishnan (2018)Yellow emitting Cd doped SnO_2 nanophosphor for phosphor converted white LED applications. Materials Sciencein Semiconductor Processing, 85, 141–149 https://doi.org/10.1016/j.mssp.2018.06.001

[34] S.P.S. Porto, P.A.Fleury,T.C.Damen (1967) Raman Spectra of TiO_2, MgF_2, ZnF_2, FeF_2, and MnF_2. Physical Reviews Journal Archive, 154,522 https://doi.org/10.1103/PhysRev.154.522

[35] J. G. Traylor, H. G. Smith, R. M. Nicklow, M. K. Wilkinson (1971) Lattice dynamics of Rutile. Physical Review B 3,3457 https://doi.org/10.1103/PhysRevB.3.3457

[36] M. H. Kuok , L. H. Lim (1990) Temperature-dependent Raman study of tin (II) chloride. Journal of Raman Spectroscopy,21, 675-677, https://doi.org/10.1002/jrs.1250211007

[37] J.Geurts, S. Rau, W. Richter, F. J.Schmitte (1984) SnO films and their oxidation to SnO_2: Raman scattering, IR reflectivity and X-ray diffraction studies. Thin Solid Films, 121, 217-225 https://doi.org/10.1016/0040-6090(84)90303-1

[38] K. Murali Krishna, M. Sharon, M. K. Mishra, V. R. Marathe (1996) Selection of optimal mixing ratios to obtain suitable photoelectrodes from mixed semiconductors using band gap calculations. ElectrochimicaActa,41,1999-2004 https://doi.org/10.1016/0013-4686(96)00004-7

[39] L.Sangaletti, L. E. Depero, B.Allieri, F.Pioselli, E.Comini (1998) Oxidation of Sn Thin Films to SnO_2. Micro-Raman Mapping and X-ray Diffraction Studies. Journal of Materials Research**,** 13,2457-2460 https://doi.org/10.1557/JMR.1998.0343

[40] R. S.Zeferino, U.Pal, R.Melendrez, H.A.Duran-Munoz, M.B.Flores (2013) Dose enhancing behavior of hydrothermally grown Eu-doped SnO_2 nanoparticles. Journal of Applied Physics*,* 113,064306-6*,* https://doi.org/10.1063/1.4790486

[41] K. Dutta, S.K.De (2007) Optical and nonlinear electrical properties of SnO_2–polyaniline nanocomposites. Materials Letters**,** 61*,* 4967–4971 https://doi.org/10.1016/j.matlet.2007.03.086

[42] G.Zhong, M.Liu (1999) Preparation of nanostructured tin oxide using a sol–gel process based on tin tetrachloride and ethylene glycol. Journal of Materials Science**,** 34*,* 3213–3219 https://doi.org/10.1023/A:1004685907751

[43] S.D. Monredon, A.Cellot, F.Ribot, C. Sanchez, L.Armelao (2002) Synthesis and characterization of crystalline tin oxide nanoparticles. Journal of Materials Chemistry*,* 12, 2396– 2400 https://doi.org/10.1039/B203049G

[44] M. A.Farrukh, B.T.Heng, R. Adnan (2010) Surfactant controlled aqueous synthesis of SnO_2nanoparticles via the hydrothermal and conventional heating methods. Turkish Journal of Chemistry,34,537–550 https://doi.org/10.3906/kim-1001-466

[45] S.Sambasivam, D.P.Joseph, J.H.Jeong, B.C. Choi, K.T.Lim (2011) Anti-ferromagnetic interactions in Er-doped SnO_2 DMS nanoparticles. Journal of Nanoparticle Research, 13, 4623-4630 https://doi.org/10.1007/s11051-011-0426-8

[46] K. N Yu, Y. Xiong, Y. Liu, C. Xiong (1997) Microstructural change of nano-SnO_2 grain assemblages with the annealing temperature. Physical Review B*, 55(4),2666–2671* https://doi:10.1103/PhysRevB.55.2666.

[47] Powder Diffraction File. Data Cards. Inorganic Section. JCPDS, Swarthmore, Pennsylvania, USA, 1987, 21–1250 https://doi.org/10.1017/s0885715600012537

[48] K.N. Yu, Y. Xiong, Y. Lin, G. Xiong (1997) Microstructural change of nano-SnO_2 grain assemblages with the annealing temperature. Phys. Rev. B, 55, 2666–2671 https://doi.org/10.1103/PhysRevB.55.2666

[49] V. V. Kissine, S. A. Voroshilov, V. V. Sysoev (1999) Oxygen flow effect on gas sensitivity properties of tin oxide film prepared by r.f. sputtering. Sensors and Actuators B, 55(1), 55–59 https://doi:10.1016/s0925-4005(99)00022-2

[50] V. D. Mote, Y.Purushotham, B. N. Dole (2012) Williamson-Hall analysis in estimation of lattice strain in nanometer-sized ZnO particles. Journal of Theoretical and Applied Physics*,* 6(1), 1-8 https://doi.org/10.1186/2251-7235-6-6

[51] A. K. Zak, W.H. Abd. Majid, M.E. Abrishami, R. Yousefi (2011) X-ray analysis of ZnO nanoparticles by Williamson–Hall and size–strain plot methods*.* Solid State Sciences, 13(1), 251–256, https://doi.org/10.1016/j.solidstatesciences.2010.11.024

[52] S.Sarkar, R. Das (2018) Shape effect on the elastic properties of Ag nanocrystals. Micro & Nano Letters**,** 13 (3),312–315 https://doi.org/10.1049/mnl.2017.0349

[53] V. S. Jahnavi, S.K. Tripathy, A. V. N. Ramalingeswara Rao (2020) Study of the Structural, Optical, Dielectric, and Magnetic Properties of Copper-Doped SnO_2 Nanoparticles. Journal of Electronic Materials, 49, 3540-3554 https://doi:10.1007/s11664-020-08028-7

[54] K. Manikandan, S. Dhanuskodi, A.R. Thomas, N.Maheswari, G. Muralidharan, D. Sastikumar (2016) Size–strain distribution analysis of SnO_2 nanoparticles and their multifunctional applications as fiber optic gas sensors,

supercapacitors, and optical limiters. RSC Advances, 6(93),90559–90570 https://doi:10.1039/c6ra20503h

[55] M. K. Singh, M. C.Mathpal, A.Agarwal (2012) Optical properties of SnO_2dots synthesized by laser ablation in liquid. Chemical Physics Letters, 536, 87-91 https://doi.org/10.1016/j.cplett.2012.03.084

[56] C. Wang, M.Ge, J.Z.Jiang (2010) Magnetic behavior of SnO_2 nanosheets at room temperature. Applied Physics Letters, 97, 042510-042510-3 https://doi.org/10.1063/1.3473764

[57] G. A. Alanko, A. Thurber, C. B. Hanna, A. Punnoose (2012) Size, surface structure, and doping effects on ferromagnetism in SnO_2. Journal of Applied Physics, 111,07C321 https://doi.org/10.1063/1.3679455

[58] P. Wu, B. Zhou, W. Zhou (2012) Room-temperature ferromagnetism in epitaxial Mg-doped SnO_2 thin films. Applied Physics Letters,100,1824051-4, https://doi.org/10.1063/1.4711220

[59] S.J.Liu, C.Y.Liu, J.Y.Juang, H.W.Fang (2009) Room-temperature ferromagnetism in Zn and MncodopedSnO2 films. Journal of Applied Physics,105,013928-1-013928-4, https://doi.org/10.1063/1.3056374

[60] H.Kimura, T.Fukumura, M.Kawasaki, K.Inaba, T.Hasegawa (2002) Rutile-type oxide-diluted magnetic semiconductor: Mn-doped SnO_2. Applied Physics Letters, 80,94-96 https://doi.org/10.1063/1.1430856

[61] S. K. Misra, S. I. Andronenko, K.M.Reddy, J.Hays, A.Punnoose (2006) Magnetic resonance studies of Co^{2+} ions in nanoparticles of SnO_2 processed at different temperatures. Journal of Applied Physics,99, 08M106, https://doi.org/10.1063/1.2165146

[62] K. M. Lee, D.J. Lee, H.Ahn (2004) XRD and TEM studies on tin oxide (II) nanoparticles prepared by inert gas condensation. Materials Letters,58,3122 – 3125, https://doi.org/10.1016/j.matlet.2004.06.002

[63] S.Das, S.Kar, S.Chaudhuri (2006) Optical properties of SnO_2 nanoparticles and nanorods synthesized by solvothermal process. Journal of Applied Physics, 99,114303-114309 https://doi.org/10.1063/1.2200449

[64] K. Vanheusden, W. L. Warren, C. H. Seager, D. R. Tallant, J. A. Voigt (1996) Mechanisms behind green photoluminescence in ZnO phosphor powders. Journal of Applied Physics, 79,7983-7990 https://doi.org/10.1063/1.362349

IZVOD

ISPITIVANJE STRUKTURNIH, OPTIČKIH I EMISIONIH SVOJSTAVA NANOČESTICA SnO_2 METODOM TERMIČKE DEKOMPOZICIJE

Nanočestice SnO_2 su sintetizovane tehnikom termičke dekompozicije variranjem temperature od 300°C do 600°C. Sintetizovane nanočestice (9 nm) su bile rutilne (tetragonalne) faze sa orijentacijom duž [110], [101], [200], [211], [220], [310], [112], [301], [202] kristalnih ravni. Maksimalni intenzitet kristalnih ravni postaje istaknut sa povećanjem temperature raspadanja dok se faze nečistoće smanjuju. Veličina kristalita i mikronaprezanje nanočestice su izračunati korišćenjem Vilijam Holove jednačine sa modelom deformacije spoja. Nanočestice SnO_2 sintetizovane na 600°C pokazuju pozitivan soj $0,3571x10^{-3}$ označava proširenje rešetke. Pri termičkoj dekompoziciji od 500 ^{0}C, uzorak ima maksimalnu transparentnost sa razmakom u pojasu od ~ 4,19eV i širokom emisijom u plavoj oblasti EM spektra sa visokim intenzitetom (5 x105 brojanja), što ga čini pogodnim za plave LED diode.

Ključne reči: *Metoda termičke razgradnje, nanočestice SnO_2, kalaj (II) hloriddihidrat*

naucni rad
rad primljen: 29.01.2025
rad korigovan: 19.02.2025.
rad prihvacen: 23.02.2025.

Amirthavalli V. https://orcid.org/0000-0002-8548-3202
Anita R. Warrier: https://orcid.org/0000-0002-1771-9586